Made available through a Creative Commons CC-BY-NC-ND License

NANO LETTERS

ACS AUTHORCHOICE

pubs.acs.org/NanoLett

Letter

Emergence of Potential-Controlled Cu-Nanocuboids and Graphene-Covered Cu-Nanocuboids under *Operando* CO_2 Electroreduction

Thanh Hai Phan, Karla Banjac, Fernando P. Cometto, Federico Dattila, Rodrigo García-Muelas, Stefan J. Raaijman, Chunmiao Ye, Marc T. M. Koper, Núria López, and Magalí Lingenfelder*

Cite This: https://dx.doi.org/10.1021/acs.nanolett.0c04703

Read Online

ACCESS | Metrics & More | Article Recommendations | Supporting Information

ABSTRACT: The electroreduction of CO_2 (CO_2RR) is a promising strategy toward sustainable fuels. Cu is the only Earth-abundant and pure metal capable of catalyzing CO_2-to-hydrocarbons conversion with significant Faradaic efficiencies; yet, its dynamic structure under *operando* CO_2RR conditions remains unknown. Here, we track the Cu structure *operando* by electrochemical scanning tunneling microscopy and Raman spectroscopy. Surprisingly, polycrystalline Cu surfaces reconstruct forming Cu nanocuboids whose size can be controlled by the polarization potential and the time employed in their *in situ* synthesis, without the assistance of organic surfactants and/or halide anions. If the Cu surface is covered by a graphene monolayer, smaller features with enhanced catalytic activity for CO_2RR can be prepared. The graphene-protecting layer softens the 3D morphological changes that Cu-based catalysts suffer when exposed to aggressive electrochemical environments and allows us to track the kinetic roughening process. This novel strategy is promising for improving Cu long-term stability, and consequently, it could be used as a platform to ultimately control product selectivity.

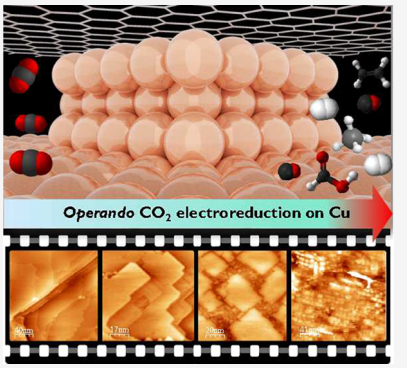

KEYWORDS: *CO_2 reduction, electrocatalysis, in situ surface reconstruction, potential-controlled roughening, graphene, copper nanocubes*

Downloaded via 67.218.250.82 on February 23, 2021 at 12:34:25 (UTC).
See https://pubs.acs.org/sharingguidelines for options on how to legitimately share published articles.

The electrochemical reduction of CO_2 (CO_2RR), via which carbon dioxide is converted to hydrocarbons, is a highly promising solution for the production of renewable fuels.[1] One of the drawbacks of this technology is that most catalysts are not selective toward energy-rich C_{2+} fuels, and therefore, their efficiencies are limited. Cu is the only Earth-abundant CO_2RR catalyst capable of converting CO_2 into hydrocarbons with significant Faradaic efficiencies.[2−4] Initial optimization toward enhanced ethylene production relies on a morphology-selectivity relationship highlighting (100) facets[5,6] as ideal geometry for C−C coupling. This reflects in an outstanding interest in the synthesis of Cu nanocuboids (CuNCs) through colloidal chemistry,[7] electrodeposition,[8] electrochemical cycling,[9] reduction of thermally grown,[10] or electrochemically grown Cu oxides and halides.[11]

However, this morphology-selectivity trend based on *ex situ*, post-mortem studies ignores the morphological evolution[12] of the catalysts during CO_2RR. Cu-based catalysts are highly dynamic: nanostructured electrocatalysts undergo fragmentation[13] and coarsening,[14] while earlier studies report on surface reconstructions[15−17] at the atomic scale on polycrystalline Cu surfaces. These morphological changes greatly affect the catalysts' long-term stability (in terms of their catalytic activity and product selectivity).[18,19] The goal of *operando* studies investigating surface dynamics is thus 3-fold: (i) to gain insight into the formation of CuNCs; (ii) to correlate *operando* surface dynamics with the trends reported in product evolution over time; (iii) to explore possible strategies for morphology conservation by, for example, covering the catalyst surface with 2D materials.[20]

In this Communication, we show the morphological transformation that polycrystalline Cu (p-Cu) and graphene-covered polycrystalline Cu (g-Cu) surfaces undergo during potentiostatic polarization at CO_2RR potentials over, at least, 4 h (Figure 1a−c). *In situ* electrochemical scanning tunneling microscopy (EC-STM) experiments reveal the dynamics of morphological evolution. Because Cu catalysts are highly prone to poisoning and deactivation during the first 30 min working at CO_2RR regimes, g-Cu represents an ideal substrate for these studies as graphene could act as a protective barrier.[21] Moreover, fresh g-Cu samples are oxide-free.[22] The thermal annealing of Cu foils under a reductive environment, performed as the pretreatment step to CVD graphene growth, results in smooth surfaces,[23] hence allowing high-resolution EC-STM imaging over an enlarged potential window.

To validate the choice of g-Cu as the model system for *operando* studies of Cu-based CO_2RR catalysts, we first

Received: November 27, 2020
Revised: February 17, 2021

© XXXX The Authors. Published by American Chemical Society

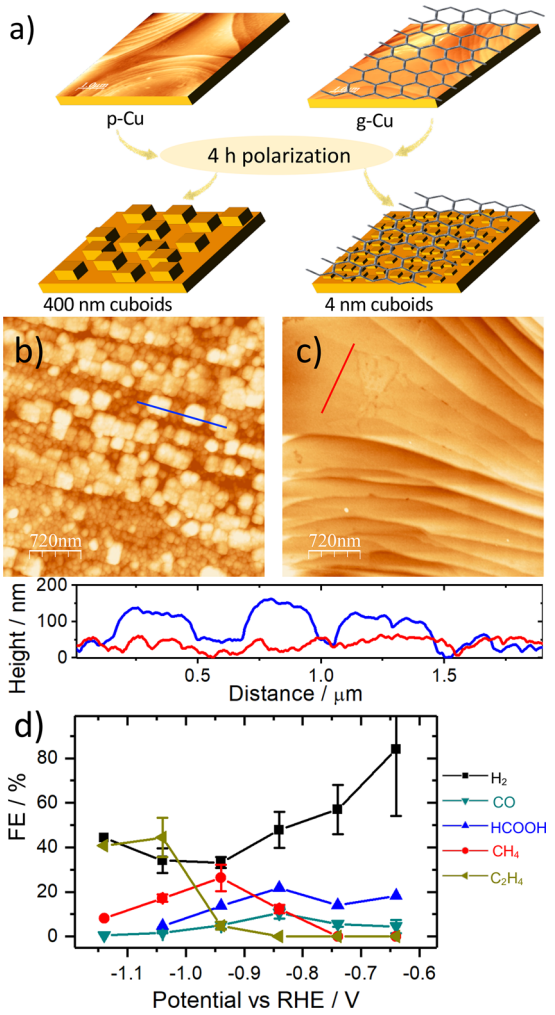

Figure 1. (a–c) Scheme and *ex situ* AFM images with corresponding height profiles showing the CuNCs formed on a pristine polycrystalline Cu-foil (p-Cu) and a graphene-covered (g-Cu) after polarization at −1 V vs a Pt pseudoreference electrode in a 0.1 M CO_2-saturated $KHCO_3$ solution for 4 h. (d) Potential-dependent product analysis on g-Cu performed using gas chromatography and high-performance liquid chromatography after chronoamperometric polarization in 0.1 M CO_2-saturated $KHCO_3$.

performed potential-dependent product analysis using gas chromatography and high-performance liquid chromatography (Figure 1d). In contrast with other graphitic-Cu electrodes, where oxygen and nitrogen defects affect the reaction pathways of CO_2RR,[24,25] we found remarkably similar trends in product selectivity on g-Cu (Figure 1d) and p-Cu earlier reported by Kuhl et al.,[4] suggesting similar CO_2RR reaction pathways on the Cu surface. Furthermore, the resemblance in CO_2RR product selectivity between g-Cu and p-Cu allows us to focus our studies on the morphological changes that both g-Cu and p-Cu undergo at CO_2RR potentials (shown in Figure 1a–c).

CuNCs, reported earlier in the literature, were synthesized by electroreduction of Cu oxide or halide films, electrodeposition, or colloidal chemistry (protected by organic surfactants).[11,10,7,9,8] To the best of our knowledge, this is the first report on CuNCs preparation by the one-step massive reconstruction of a Cu surface to cuboids, that are up to 400 nm in width, upon 4 h potentiostatic polarization in a halide-free electrolyte. Here, CuNCs growth during CO_2RR is related to a surface reconstruction mainly governed by the polarization of the substrate, in agreement with the reports on surface reconstructions of p-Cu to Cu(100).[15,17] In order to exclude the role of CO_2 on the mechanism of CuNC formation, the same preparation protocol was conducted in an electrolyte saturated with N_2: similar CuNCs were observed (Figure S2). This further supports that surface reconstruction leading to CuNC formation after prolonged exposure is mainly driven by interfacial polarization.

To gain knowledge on the surface reconstruction dynamics, we performed a series of *in situ* EC-STM experiments to follow the transformation of the p-Cu surface underneath graphene. STM offers the unique possibility to monitor preferentially either the graphene layer or the Cu surface underneath by changing the STM bias conditions (Figure 2a). The EC-polarization potential, located at a more negative value than the Cu_xO reduction potentials, is kept constant at the positive edge of CO_2RR and the hydrogen evolution reaction (HER) regime to avoid bubble evolution and interference of the Faradaic currents (crucial for *in situ* EC-STM experiments). A dynamic observation of the different stages of the surface nanostructuring was followed by *in situ* EC-STM on g-Cu (Figures 2b–i and S3). The initial stages of this process (Figure 2b–d) show how the polycrystalline Cu underneath the graphene is initially reconstructed to Cu mesocrystals within the first hour. Then, further reconstruction leads to formation of a few nanometers-wide Cu(100) facets (Figure 2e, f). Figure 2f′ shows that the graphene layer is still present during this reconstruction.

Small cuboid-features gradually grow on top of the Cu(100) facets; their size is gradually reducing as a function of time (as seen in Figures 2g–i), reaching an average edge length of ca. 4 ± 1 nm after 4 h of polarization. The CuNCs size and the kinetics of formation can be tuned by changing the potentiostatic polarization time or applying more negative potential values (the more negative the potential value, the smaller the cuboids and the shorter the time employed to appear, Figure S5). Density functional theory (DFT) modeling supports that surface reconstruction is mostly driven by surface polarization, see Supporting Discussion 6. Open facets such as Cu(100) store electrostatic energy more effectively than Cu(111) due to the low coordination of surface Cu atoms (Figures S6 and S7); therefore, at very negative potentials, they are more stable than the closed-packed domains (Figure S8). By having a shorter principal radius of curvature, smaller structures experience a higher electric potential across them than flat surroundings; thus, they undergo further reconstruction toward nanocuboid features with even lower Cu coordination. The role of adsorbed species, in particular H, was not explored in this model; therefore, we cannot discard that they might play a synergetic role in this process.[26]

Operando Raman spectra (Figure 2j) show the absence of native copper oxides during the morphological evolution. The peaks attributed to Cu_xO species[27,28] (~410–500 cm^{-1} for Cu_2O and ~621 cm^{-1} for CuO, respectively) disappear at the beginning of reconstruction, indicating that the native oxide layer present in air-exposed g-Cu surfaces was fully reduced (see more details in Supplementary Discussion 4).[29] This is in agreement with our EC-STM measurements showing smooth metallic Cu terraces (Figure 2b–i).

Interestingly, the graphene remains almost invariant on top of the as-prepared CuNCs (Figures 2j and S4). Figure 3a, b shows *ex situ* STM images of g-Cu surfaces before and after EC

https://dx.doi.org/10.1021/acs.nanolett.0c04703
Nano Lett. XXXX, XXX, XXX−XXX

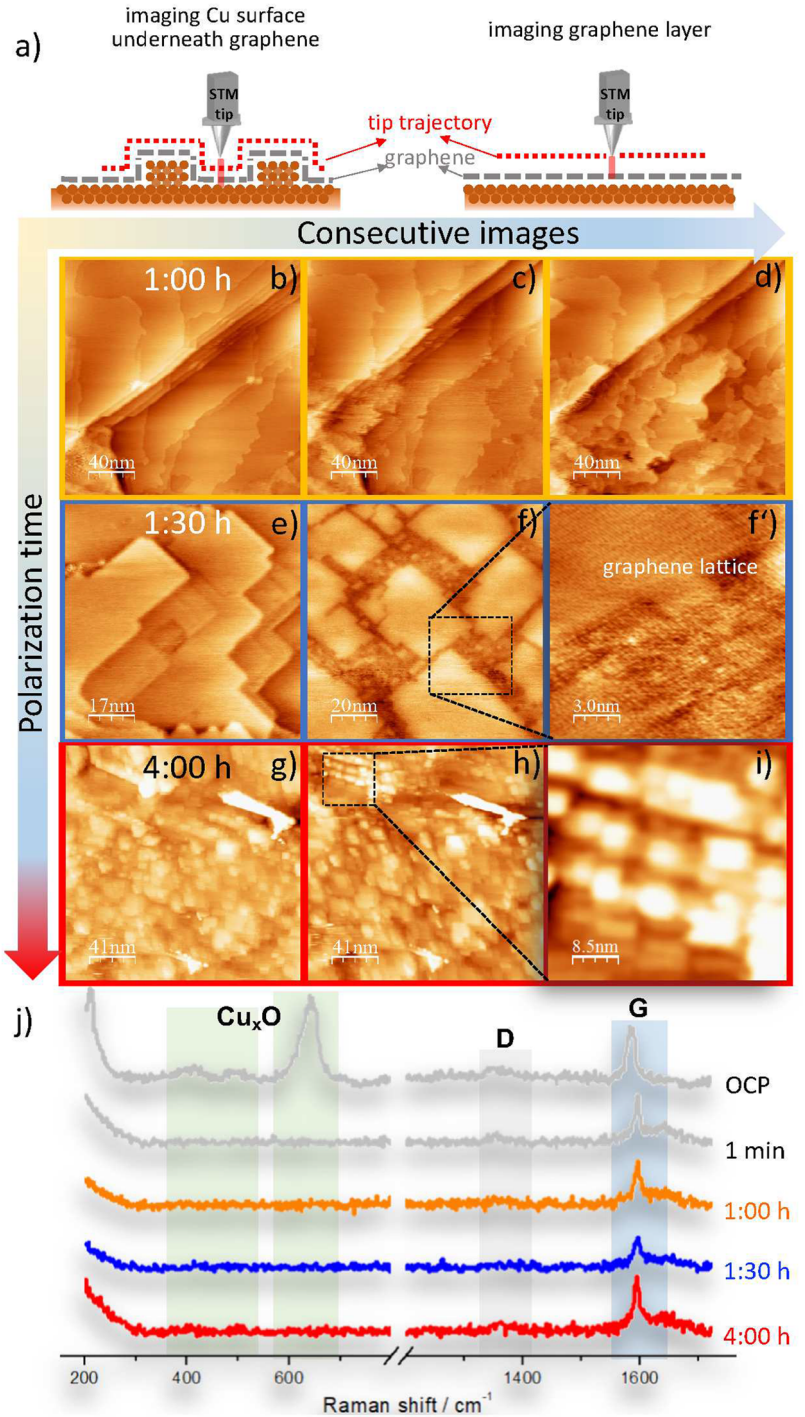

Figure 2. (a) Schemes illustrating STM imaging of g-Cu: by changing the STM scanning parameters, we visualize either the Cu surface underneath graphene or the atomic lattice of the graphene overlayer. (b–i) Series of EC-STM images showing the morphological evolution of a g-Cu surface during CO_2RR in 0.1 M CO_2-saturated $KHCO_3$: (b–f) from polycrystalline Cu to Cu(100) facets and (g–i) to nanocuboids. U_{cell} = −1.0 V vs Pt pseudo-RE, U_{bias} = 328 mV, I = 1.75 nA. (f′) Atomic lattice of the graphene overlayer recorded on top of Cu(100) facets confirming the presence of graphene during reconstruction. (j) *Operando* Raman spectra of g-Cu obtained during reconstruction, illustrated in EC-STM images from panels b–i, showing the immediate reduction of native Cu_xO to metallic Cu and the presence of graphene during CuNC formation on g-Cu.

treatment, respectively. It can be observed that the hexagonal lattice of graphene is still present on top of the CuNCs. This suggests that the graphene layer remains intact during the *in situ* synthesis of the NCs. The persistence of the graphene layer was also confirmed by both *operando* (Figure 2j) and *ex situ* Raman spectroscopy (Figure 3c), where *ex situ* spectra were collected on the same g-Cu sample before and after CuNC formation. All spectra exhibit typical graphene peaks at ∼1591 cm^{-1} (the G band) and ∼2721 cm^{-1} (the 2D band).[30] The absence of the D band (∼1350 cm^{-1}) on all spectra confirms the presence of a defect-free graphene layer before (i.e., on pristine g-Cu), during and after CuNC formation. This further confirms that the as-formed CuNCs are covered with graphene (g-CuNCs).

https://dx.doi.org/10.1021/acs.nanolett.0c04703
Nano Lett. XXXX, XXX, XXX−XXX

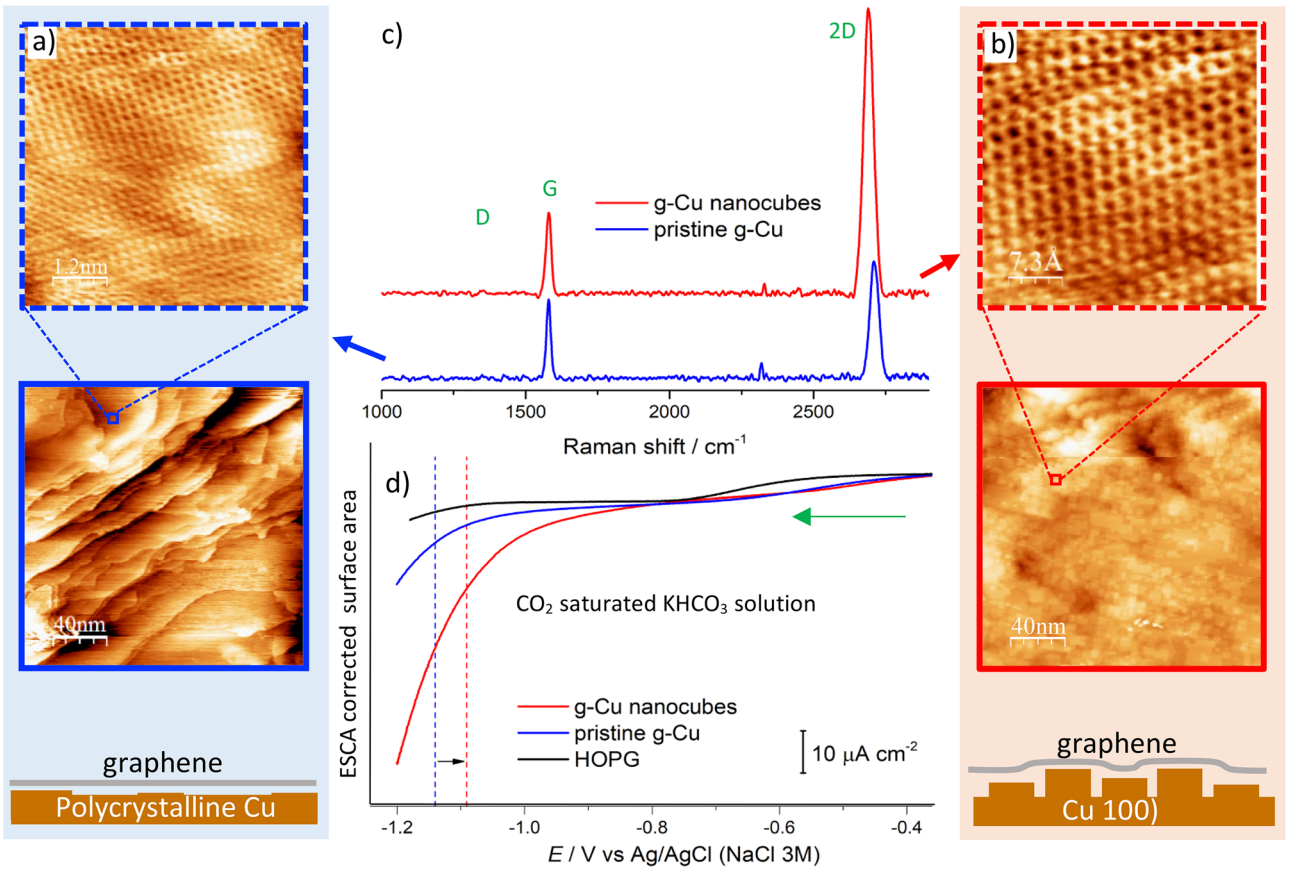

Figure 3. *Ex situ* STM images showing graphene (a) before and (b) after reconstruction to g-CuNCs. U_{bias} = 0.1 mV, I = 10.5 nA. (c) *Ex situ* Raman spectra of pristine g-Cu and g-CuNCs. The gray band highlights the wavenumber where the D band is usually observed. (d) ECSA-corrected linear sweep voltammograms obtained for pristine g-Cu, g-CuNCs, and HOPG.

Following the same procedure, similar scenarios were observed on p-Cu. That is, initially, polycrystalline Cu evolves gradually to mesocrystals, Cu(100) facets, and cuboids (Figure S9). These results indicate that different Cu surfaces form nanocuboids after prolonged exposition to CO_2RR potentials (e.g., Cu foil, polished Cu, g-Cu, Cu functionalized with molecular additives,[31] etc.).

Even if the cuboid structures once formed conserve their morphology *ex situ* at least for several days (Figure 1b, c), a detailed analysis of the first steps in the formation of nanocuboid features points toward a kinetic roughening process, where multiterrace islands (five-layered mounds, Figure S10) arise as a consequence of step-edge (Ehrlich–Schwoebel or ES) barriers,[32,33] inhibiting downward transport of adatoms.

The fact that these are far-from-equilibrium structures is consistent with the sharp and straight step edges (Figure S10) along [010] and [001] Cu(001) directions, in contrast to the edge-rounded equilibrium structures seen after homoepitaxy of Cu on Cu(001).[34,35] Moreover, the absence of fuzzy g-CuNCs step edges points toward the absence of adsorbates at the Cu edges during the potential-driven roughening process (see Supplementary Discussion 5 for more details). The formation of g-CuNCs happens underneath graphene (as shown in Figure 1c and illustrated in Figures 1a and 2a) during CO_2RR at negative potentials, at which no redeposition of electrochemically dissolved atoms is expected.[36] Therefore, the adatoms nucleating in the upper terraces might originate and diffuse from the grain boundaries. Further studies looking at the kinetics of the process under different electrolytes and pH conditions are underway to assess if potential-driven reconstructions[37] as a kinetic phenomenon might be a general explanation for surface transformations observed on Cu and other metals during HER/CO_2RR.[38]

Finally, we performed a preliminary study comparing the CO_2RR/HER performance of the g-CuNCs to a highly-oriented pyrolytic graphite (HOPG) substrate (as a representative model system of the graphene layer) and to a pristine g-Cu sample. Linear sweep voltammograms corrected for the electrochemically active surface area (ECSA) in a 0.1 M CO_2-saturated $KHCO_3$ are shown in Figure 3d. At negative potentials, cathodic current densities increase exponentially due to the CO_2RR and the parasitic HER. This effect is especially pronounced for g-CuNCs, where the presence of CuNCs underneath graphene leads to a shift in the HER/CO_2RR onset potentials to more positive values and increases the current density more than twice compared to the pristine g-Cu sample. These preliminary experiments hint that as-prepared g-CuNCs could show an enhanced HER/CO_2RR performance due to the unique combination of the (100) facets and confinement effects[39,40] at the Cu/graphene interface.

In conclusion, we show that Cu surfaces suffer a drastic reconstruction under long exposure to negative potentials, evolving from polycrystalline Cu to nanocuboids, even in halide-free electrolytes. To prevent this massive reconstruction under *operando* conditions, we demonstrate the protective character of a single graphene layer on the Cu catalysts. The

https://dx.doi.org/10.1021/acs.nanolett.0c04703
Nano Lett. XXXX, XXX, XXX−XXX

size of the nanocuboids can be tuned by the applied potential and/or the polarization time; e.g., 4 ±1 nm g-CuNCs can be prepared after 4 h of polarization at −1 V vs Pt pseudo-RE. A dynamic observation of the gradual surface reconstruction from polycrystalline Cu to nanocuboids is reported by *in situ* EC-STM. As STM measurements cannot be performed in massively reconstructed Cu, this model system is ideal for *in situ* studies. By both *operando* and *ex situ* Raman spectroscopy, we show that the graphene layer on g-Cu remains intact during this process. This study opens new avenues to reinterpret the mechanism of nanostructured Cu-based materials without the presence of oxidized Cu species nor halides. In particular, it sheds light on the fact that Cu catalysts, when normalized by the electrochemically active surface area, show similar intrinsic activity;[38] most likely because the surface morphology (although highly dynamic) and step density under *operando* conditions are very similar at the atomic scale: the scale where ultimately CO_2RR occurs.

■ ASSOCIATED CONTENT

Supporting Information

The Supporting Information is available free of charge at https://pubs.acs.org/doi/10.1021/acs.nanolett.0c04703.

Experimental details and additional data, AFM images, EC-STM images, Raman spectra, electrostatic energy, modeled surface energies, capacitive scans, and supporting discussions (PDF)

■ AUTHOR INFORMATION

Corresponding Author

Magalí Lingenfelder − *Max Planck-EPFL Laboratory for Molecular Nanoscience and Technology and IPHYS, École Polytechnique Fédérale de Lausanne (EPFL), 1015 Lausanne, Switzerland;* orcid.org/0000-0003-1362-8879; Email: magali.lingenfelder@epfl.ch

Authors

Thanh Hai Phan − *Max Planck-EPFL Laboratory for Molecular Nanoscience and Technology and IPHYS, École Polytechnique Fédérale de Lausanne (EPFL), 1015 Lausanne, Switzerland*

Karla Banjac − *Max Planck-EPFL Laboratory for Molecular Nanoscience and Technology and IPHYS, École Polytechnique Fédérale de Lausanne (EPFL), 1015 Lausanne, Switzerland;* orcid.org/0000-0001-7063-6213

Fernando P. Cometto − *Max Planck-EPFL Laboratory for Molecular Nanoscience and Technology and IPHYS, École Polytechnique Fédérale de Lausanne (EPFL), 1015 Lausanne, Switzerland*

Federico Dattila − *Institute of Chemical Research of Catalonia (ICIQ), The Barcelona Institute of Science and Technology (BIST), 43007 Tarragona, Spain;* orcid.org/0000-0001-8195-3951

Rodrigo García-Muelas − *Institute of Chemical Research of Catalonia (ICIQ), The Barcelona Institute of Science and Technology (BIST), 43007 Tarragona, Spain;* orcid.org/0000-0002-2219-5027

Stefan J. Raaijman − *Leiden Institute of Chemistry, Leiden University, 23000 RA Leiden, The Netherlands*

Chunmiao Ye − *Leiden Institute of Chemistry, Leiden University, 23000 RA Leiden, The Netherlands*

Marc T. M. Koper − *Leiden Institute of Chemistry, Leiden University, 23000 RA Leiden, The Netherlands;* orcid.org/0000-0001-6777-4594

Núria López − *Institute of Chemical Research of Catalonia (ICIQ), The Barcelona Institute of Science and Technology (BIST), 43007 Tarragona, Spain;* orcid.org/0000-0001-9150-5941

Complete contact information is available at: https://pubs.acs.org/10.1021/acs.nanolett.0c04703

Author Contributions

T.H.P. and K.B. contributed equally. T.H.P., K.B., and M.L. designed the experiments. T.H.P. and K.B. performed the EC-STM experiments. T.H.P., K.B., and F.C. analyzed the data. K.B. performed Raman experiments and analyzed the Raman data. F.D., R.G.-M., and N.L. performed the DFT calculations. T.H.P., K.B., S.J.R., and C.Y. performed product analysis under the supervision of M.T.M.K. K.B., T.H.P., F.C., and M.L. cowrote the manuscript. All authors discussed the results and commented on the manuscript.

Notes

The data sets generated are available in the ioChem-BD database[41] at DOI: 10.19061/iochem-bd-1-185.

The authors declare no competing financial interest.

■ ACKNOWLEDGMENTS

We acknowledge EPFL technical and scientific support from Dr. Arnaud Magrez, Dr. Astrid Olaya Avendano, Dr. Gian Luca De Gregorio, Prof. Raffaella Buonsanti, Dr. Natalia Gasilova, and Dr. Daniel Ortiz during the initial setup of this project. This work has received funding from the European Union's Horizon 2020 research and innovation program under grant agreement no. 732840 A-LEAF. F.D., R.G.-M., and N.L. additionally acknowledge funding from the European Union's Horizon 2020 research and innovation program under grant agreement no. 722614 ELCOREL and from the Spanish Ministry of Science and Innovation (grant no. RTI2018-101394−B-I00) and BSC-RES for generous computational resources.

■ ABBREVIATIONS

AFM, atomic force microscopy; CO_2RR, electrochemical reductive reaction of carbon dioxide; CuNCs, copper nanocuboids; CVD, chemical vapor deposition; ECSA, electrochemically active surface area; EC-STM, electrochemical scanning tunneling microscopy; g-Cu, graphene-covered copper; g-CuNCs, graphene-covered copper nanocuboids; HOPG, highly oriented pyrolytic graphite; p-Cu, polycrystalline copper; RE, reference electrode; STM, scanning tunneling microscopy

■ REFERENCES

(1) Lim, X. How to Make the Most of Carbon Dioxide. *Nature* **2015**, *526* (7575), 628.

(2) Hori, Y.; Murata, A.; Takahashi, R.; Suzuki, S. Enhanced Formation of Ethylene and Alcohols at Ambient Temperature and Pressure in Electrochemical Reduction of Carbon Dioxide at a Copper Electrode. *J. Chem. Soc., Chem. Commun.* **1988**, No. 1, 17−19.

(3) Peterson, A. A.; Abild-Pedersen, F.; Studt, F.; Rossmeisl, J.; Nørskov, J. K. How Copper Catalyzes the Electroreduction of Carbon Dioxide into Hydrocarbon Fuels. *Energy Environ. Sci.* **2010**, *3* (9), 1311−1315.

(4) Kuhl, K. P.; Cave, E. R.; Abram, D. N.; Jaramillo, T. F. New Insights into the Electrochemical Reduction of Carbon Dioxide on Metallic Copper Surfaces. *Energy Environ. Sci.* **2012**, *5* (5), 7050−7059.
(5) Hori, Y.; Murata, A.; Takahashi, R.; Suzuki, S. Electroreduction of Carbon Monoxide to Methane and Ethylene at a Copper Electrode in Aqueous Solutions at Ambient Temperature and Pressure. *J. Am. Chem. Soc.* **1987**, *109* (16), 5022−5023.
(6) Bagger, A.; Ju, W.; Varela, A. S.; Strasser, P.; Rossmeisl, J. Electrochemical CO_2 Reduction: Classifying Cu Facets. *ACS Catal.* **2019**, *9* (9), 7894−7899.
(7) Loiudice, A.; Lobaccaro, P.; Kamali, E. A.; Thao, T.; Huang, B. H.; Ager, J. W.; Buonsanti, R. Tailoring Copper Nanocrystals towards C_2 Products in Electrochemical CO_2 Reduction. *Angew. Chem., Int. Ed.* **2016**, *55* (19), 5789−5792.
(8) Wang, Y.; Wang, Z.; Dinh, C.-T.; Li, J.; Ozden, A.; Golam Kibria, M.; Seifitokaldani, A.; Tan, C.-S.; Gabardo, C. M.; Luo, M.; Zhou, H.; Li, F.; Lum, Y.; McCallum, C.; Xu, Y.; Liu, M.; Proppe, A.; Johnston, A.; Todorovic, P.; Zhuang, T.-T.; Sinton, D.; Kelley, S. O.; Sargent, E. H. Catalyst Synthesis under CO_2 Electroreduction Favours Faceting and Promotes Renewable Fuels Electrosynthesis. *Nat. Catal.* **2020**, *3* (2), 98−106.
(9) Kwon, Y.; Lum, Y.; Clark, E. L.; Ager, J. W.; Bell, A. T. CO_2 Electroreduction with Enhanced Ethylene and Ethanol Selectivity by Nanostructuring Polycrystalline Copper. *ChemElectroChem* **2016**, *3* (6), 1012−1019.
(10) Kas, R.; Kortlever, R.; Yılmaz, H.; Koper, M. T. M.; Mul, G. Manipulating the Hydrocarbon Selectivity of Copper Nanoparticles in CO_2 Electroreduction by Process Conditions. *ChemElectroChem* **2015**, *2* (3), 354−358.
(11) Chen, C. S.; Handoko, A. D.; Wan, J. H.; Ma, L.; Ren, D.; Yeo, B. S. Stable and Selective Electrochemical Reduction of Carbon Dioxide to Ethylene on Copper Mesocrystals. *Catal. Sci. Technol.* **2015**, *5* (1), 161−168.
(12) Kim, D.; Kley, C. S.; Li, Y.; Yang, P. Copper Nanoparticle Ensembles for Selective Electroreduction of CO_2 to C_2−C_3 Products. *Proc. Natl. Acad. Sci. U. S. A.* **2017**, *114* (40), 10560−10565.
(13) Jung, H.; Lee, S. Y.; Lee, C. W.; Cho, M. K.; Won, D. H.; Kim, C.; Oh, H.-S.; Min, B. K.; Hwang, Y. J. Electrochemical Fragmentation of Cu_2O Nanoparticles Enhancing Selective C-C Coupling from CO_2 Reduction Reaction. *J. Am. Chem. Soc.* **2019**, *141*, 4624.
(14) Huang, J.; Hormann, N.; Oveisi, E.; Loiudice, A.; De Gregorio, G. L.; Andreussi, O.; Marzari, N.; Buonsanti, R. Potential-Induced Nanoclustering of Metallic Catalysts during Electrochemical CO_2 Reduction. *Nat. Commun.* **2018**, *9* (1), 3117.
(15) Kim, Y.-G.; Baricuatro, J. H.; Javier, A.; Gregoire, J. M.; Soriaga, M. P. The Evolution of the Polycrystalline Copper Surface, First to Cu(111) and Then to Cu(100), at a Fixed CO_2RR Potential: A Study by *Operando* EC-STM. *Langmuir* **2014**, *30* (50), 15053−15056.
(16) Gunathunge, C. M.; Li, X.; Li, J.; Hicks, R. P.; Ovalle, V. J.; Waegele, M. M. Spectroscopic Observation of Reversible Surface Reconstruction of Copper Electrodes under CO_2 Reduction. *J. Phys. Chem. C* **2017**, *121* (22), 12337−12344.
(17) Kim, Y.-G.; Baricuatro, J. H.; Soriaga, M. P. Surface Reconstruction of Polycrystalline Cu Electrodes in Aqueous $KHCO_3$ Electrolyte at Potentials in the Early Stages of CO_2 Reduction. *Electrocatalysis* **2018**, *9*, 526−530.
(18) Grosse, P.; Gao, D.; Scholten, F.; Sinev, I.; Mistry, H.; Roldan Cuenya, B. Dynamic Changes in the Structure, Chemical State and Catalytic Selectivity of Cu Nanocubes during CO_2 Electroreduction: Size and Support Effects. *Angew. Chem., Int. Ed.* **2018**, *57* (21), 6192−6197.
(19) Moller, T.; Scholten, F.; Thanh, T. N.; Sinev, I.; Timoshenko, J.; Wang, X.; Jovanov, Z.; Gliech, M.; Roldan Cuenya, B.; Varela, A. S.; Strasser, P. Electrocatalytic CO_2 Reduction on CuO_x Nanocubes: Tracking the Evolution of Chemical State, Geometric Structure, and Catalytic Selectivity Using Operando Spectroscopy. *Angew. Chem., Int. Ed.* **2020**, *59* (41), 17974−17983.
(20) Li, Y.; Cui, F.; Ross, M. B.; Kim, D.; Sun, Y.; Yang, P. Structure-Sensitive CO_2 Electroreduction to Hydrocarbons on Ultrathin 5-Fold Twinned Copper Nanowires. *Nano Lett.* **2017**, *17* (2), 1312−1317.
(21) Hong, J.; Lee, S.; Lee, S.; Han, H.; Mahata, C.; Yeon, H.-W.; Koo, B.; Kim, S.-I.; Nam, T.; Byun, K.; Min, B.-W.; Kim, Y.-W.; Kim, H.; Joo, Y.-C.; Lee, T. Graphene as an Atomically Thin Barrier to Cu Diffusion into Si. *Nanoscale* **2014**, *6* (13), 7503−7511.
(22) Chen, S.; Brown, L.; Levendorf, M.; Cai, W.; Ju, S.-Y.; Edgeworth, J.; LI, X.; Manguson, C. W.; Velamakanni, A.; Pinert, R. D.; Kang, J.; Park, J.; Ruoff, R. S. Oxidation Resistance of Graphene-Coated Cu and Cu/Ni Alloy. *ACS Nano* **2011**, *5* (2), 1321−1327.
(23) Kim, S. M.; Hsu, A.; Lee, Y.-H.; Dresselhaus, M.; Palacios, T.; Kim, K. K.; Kong, J. The Effect of Copper Pre-Cleaning on Graphene Synthesis. *Nanotechnology* **2013**, *24* (36), 365602.
(24) Song, Y.; Peng, R.; Hensley, D. K.; Bonnesen, P. V.; Liang, L.; Wu, Z.; Meyer, H. M.; Chi, M.; Ma, C.; Sumpter, B. G.; Rondinone, A. J. High-Selectivity Electrochemical Conversion of CO_2 to Ethanol Using a Copper Nanoparticle/N-Doped Graphene Electrode. *ChemistrySelect* **2016**, *1* (19), 6055−6061.
(25) Geioushy, R. A.; Khaled, M. M.; Hakeem, A. S.; Alhooshani, K.; Basheer, C. High Efficiency Graphene/Cu_2O Electrode for the Electrochemical Reduction of Carbon Dioxide to Ethanol. *J. Electroanal. Chem.* **2017**, *785*, 138−143.
(26) McCrum, I. T.; Bondue, C. J.; Koper, M. T. M. Hydrogen-Induced Step-Edge Roughening of Platinum Electrode Surfaces. *J. Phys. Chem. Lett.* **2019**, *10* (21), 6842−6849.
(27) Yin, X.; Li, Y.; Ke, F.; Lin, C.; Zhao, H.; Gan, L.; Luo, Z.; Zhao, R.; Heinz, T. F.; Hu, Z. Evolution of the Raman Spectrum of Graphene Grown on Copper upon Oxidation of the Substrate. *Nano Res.* **2014**, *7* (11), 1613−1622.
(28) Lee, U.; Han, Y.; Lee, S.; Kim, J. S.; Lee, Y. H.; Kim, U. J.; Son, H. Time Evolution Studies on Strain and Doping of Graphene Grown on a Copper Substrate Using Raman Spectroscopy. *ACS Nano* **2020**, *14* (1), 919−926.
(29) Scott, S. B.; Hogg, T. V.; Landers, A. T.; Maagaard, T.; Bertheussen, E.; Lin, J. C.; Davis, R. C.; Beeman, J. W.; Higgins, D.; Drisdell, W. S.; Hahn, C.; Mehta, A.; Seger, B.; Jaramillo, T. F.; Chorkendorff, I. Absence of Oxidized Phases in Cu under CO Reduction Conditions. *ACS Energy Lett.* **2019**, *4* (3), 803−804.
(30) Costa, S. D.; Righi, A.; Fantini, C.; Hao, Y.; Magnuson, C.; Colombo, L.; Ruoff, R. S.; Pimenta, M. A. Resonant Raman Spectroscopy of Graphene Grown on Copper Substrates. *Solid State Commun.* **2012**, *152* (15), 1317−1320.
(31) Thevenon, A.; Rosas-Hernández, A.; Peters, J. C.; Agapie, T. In-Situ Nanostructuring and Stabilization of Polycrystalline Copper by an Organic Salt Additive Promotes Electrocatalytic CO_2 Reduction to Ethylene. *Angew. Chem., Int. Ed.* **2019**, *58* (47), 16952−16958.
(32) Schwoebel, R. L.; Shipsey, E. J. Step Motion on Crystal Surfaces. *J. Appl. Phys.* **1966**, *37*, 3682−3686.
(33) Ehrlich, G.; Hudda, F. G. Atomic View of Surface Self-Diffusion: Tungsten on Tungsten. *J. Chem. Phys.* **1966**, *44* (3), 1039−1049.
(34) Girard, J. C.; Samson, Y.; Gauthier, S.; Roussel, S.; Klein, J. STM Study of the Nucleation and Annealing of Ion Bombardment Induced Defects on Cu(100). *Surf. Sci.* **1994**, *302* (1), 73−80.
(35) Hannon, J. B.; Klünker, C.; Giesen, M.; Ibach, H.; Bartelt, N. C.; Hamilton, J. C. Surface Self-Diffusion by Vacancy Motion: Island Ripening on Cu(001). *Phys. Rev. Lett.* **1997**, *79* (13), 2506−2509.
(36) Speck, F. D.; Cherevko, S. Electrochemical Copper Dissolution: A Benchmark for Stable CO_2 Reduction on Copper Electrocatalysts. *Electrochem. Commun.* **2020**, *115*, 106739.
(37) Dakkouri, A. S.; Kolb, D. M. Reconstruction of Gold Surfaces. In *Interfacial Electrochemistry: Theory, Experiments, and Applications*; Wieckowski, A., Ed.; Marcel Dekker Inc.: New York, 1999; pp 151−173.
(38) Nitopi, S.; Bertheussen, E.; Scott, S. B.; Liu, X.; Engstfeld, A. K.; Horch, S.; Seger, B.; Stephens, I. E. L.; Chan, K.; Hahn, C.; Nørskov, J. K.; Jaramillo, T. F.; Chorkendorff, I. Progress and Perspectives of

https://dx.doi.org/10.1021/acs.nanolett.0c04703
Nano Lett. XXXX, XXX, XXX−XXX

Electrochemical CO_2 Reduction on Copper in Aqueous Electrolyte. *Chem. Rev.* **2019**, *119*, 7610.
(39) Li, H.; Xiao, J.; Fu, Q.; Bao, X. Confined Catalysis under Two-Dimensional Materials. *Proc. Natl. Acad. Sci. U. S. A.* **2017**, *114* (23), 5930−5934.
(40) Wordsworth, J.; Benedetti, T. M.; Alinezhad, A.; Tilley, R. D.; Edwards, M. A.; Schuhmann, W.; Gooding, J. J. The Importance of Nanoscale Confinement to Electrocatalytic Performance. *Chem. Sci.* **2020**, *11* (5), 1233−1240.
(41) Álvarez-Moreno, M.; de Graaf, C.; López, N.; Maseras, F.; Poblet, J. M.; Bo, C. Managing the Computational Chemistry Big Data Problem: The IoChem-BD Platform. *J. Chem. Inf. Model.* **2015**, *55* (1), 95−103.

https://dx.doi.org/10.1021/acs.nanolett.0c04703
Nano Lett. XXXX, XXX, XXX−XXX